


Improving Short-Term Stability in Optical Lattice Clocks by Quantum Nondemolition Measurement

Daniel Benedicto Orenes,¹ Robert J. Sewell,¹ Jérôme Lodewyck^{ORCID},² and Morgan W. Mitchell^{1,3}

¹*ICFO—Institut de Ciències Fotòniques, The Barcelona Institute of Science and Technology, 08860 Castelldefels (Barcelona), Spain*

²*LNE–SYRTE, Observatoire de Paris, Université PSL, CNRS, Sorbonne Université, 61 avenue de l’Observatoire, F-75014 Paris, France*

³*ICREA—Institució Catalana de Recerca i Estudis Avançats, 08010 Barcelona, Spain*

 (Received 22 October 2021; revised 20 March 2022; accepted 23 March 2022; published 13 April 2022)

We propose a multimeasurement estimation protocol for quantum nondemolition (QND) measurements in a Rabi clock interferometer. The method is well suited for current state-of-the-art optical lattice clocks with QND measurement capabilities. The protocol exploits the correlations between multiple non-destructive measurements of the initially prepared coherent spin state. A suitable Gaussian estimator for the clock laser detuning is presented, and an analytic expression for the sensitivity of the protocol is derived. We use this analytic expression to optimize the protocol using available experimental parameters, achieving an improvement of 7.9 dB with respect to the standard quantum limit in terms of clock stability. We also discuss the measurement back-action effects of our protocol into the atomic state.

DOI: [10.1103/PhysRevLett.128.153201](https://doi.org/10.1103/PhysRevLett.128.153201)

Optical lattice clocks (OLCs) use ultranarrow (mHz) transition lines in neutral atoms as absolute frequency references and have demonstrated fractional frequency instability below 10^{-18} [1,2], enabling new applications and fundamental studies in physics [3–6]. The Dick effect (DE), i.e., the sampling of the local oscillator frequency noise by the clock interrogation sequence, remains a main contributor to the instability of OLCs [7]. However, with the observation of second-scale atomic coherence times [1,8], and with the design of measurement sequences [2,9–12] able to evade the DE, OLC short-term instability, i.e., for integration time for which readout noise or DE contributes more than residual fluctuations of systematic effects, may soon be dominated by quantum projection noise (QPN). At that point, the instability of OLCs can be further reduced using techniques from quantum optics and cavity quantum electrodynamics (CQED) [13,14].

Quantum nondemolition (QND) measurements of atomic spin [15], which produce spin squeezing [16–19], can reduce QPN as part of back-action evading measurement protocols [20–23], permit reuse of the spin ensemble to reduce dead time and the DE [12], and are compatible with more sophisticated strategies to evade the DE using multiple ensembles and synchronous measurements [2,9–11] and improve phase locking of the local oscillator [24–26]. Their efficacy is greatly enhanced using CQED methods [27,28] especially when optical lattice and cavity modes are structured to produce uniform coupling [19]. Existing and in-development OLCs incorporate optical cavities for cavity-enhanced nondestructive measurement [29–31] and multimode probing to achieve uniform coupling [31],

making them very attractive systems for quantum noise reduction.

Paradigmatic QND-based enhancement protocols [17,32–34] detect a population difference, e.g., the pseudospin component $\hat{J}_z = (\hat{N}_\uparrow - \hat{N}_\downarrow)/2$, where \hat{N}_\uparrow and \hat{N}_\downarrow are clock transition level populations. Such protocols have been successfully implemented in microwave clocks [19,25,27,28,35], but are not directly applicable to the OLC scenario, where only the ground state population \hat{N}_\downarrow is readily available to dispersive measurement [12,31,36] (see, however, Meiser *et al.* [37] for a proposal for differential population QND via far-off-resonance probing). Spin-squeezing generated on a microwave transition has also been transferred coherently to an optical clock transition [38].

Here we propose a novel protocol that uses multiple QND measurements of the ground state population \hat{N}_\downarrow of the clock transition to overcome the QPN and reduce the noise of laser detuning estimates obtained in Rabi spectroscopy. The method is thus directly applicable to state-of-the-art OLCs as presently employed. We describe the quantum and classical statistics of atoms and probe light to the second order, to obtain analytic results and optimization under several scenarios within the Gaussian approximation. For realistic QND detection parameters in current OLCs, we predict the generation of squeezed states and a metrological improvement of 7.9 dB relative to the best possible frequency stability with projective measurements.

Definition of the problem.—As illustrated in Fig. 1, we consider an ensemble of N three-level systems, in which

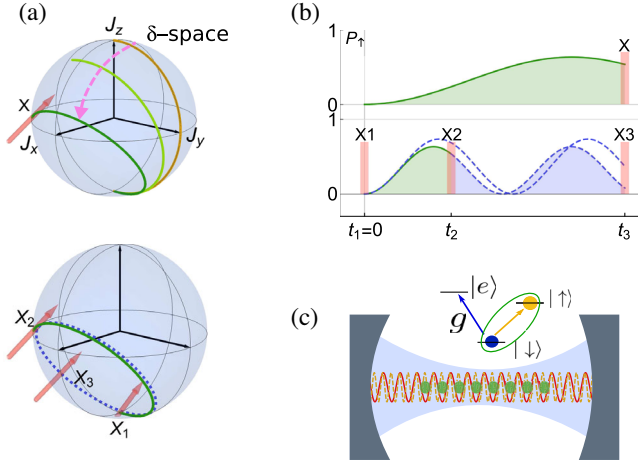


FIG. 1. (a) Bloch-sphere representation of protocols. Upper panel: reference Rabi sequence used in state-of-the-art OLCs, with a single measurement (labeled X) at the end of the sequence, used to define the SQL. The colored lines correspond to different detunings, with the dark green line corresponding to the detuning maximizing the sensitivity of the clock, and the red arrows indicate when the measurement is made. Lower panel: protocol with three QND measurements. The sensitivity of this protocol is shown as the red curve in Fig. 2. (b) Upper and lower panels: excited state population P_{\uparrow} of typical Rabi (three-measurement) protocol [green (blue)] as a function of time. Red bars indicate the timing of the QND measurements. The Rabi frequency and detuning have been adjusted such that the total interrogation time remains the same as in both protocols. The two dashed blue lines in the lower panel correspond to slightly different detunings to illustrate the sensitivity of the protocol to the detuning of the clock laser. (c) Pictorial representation of the experimental situation, showing trapping light (red), clock laser light (yellow) for inducing Rabi oscillations between $|\downarrow\rangle^{\otimes N} \leftrightarrow |\uparrow\rangle^{\otimes N}$, and probing light (light blue) coupling $|\downarrow\rangle, |e\rangle$ to nondestructively measure the ground state population. The generic representation of the energy levels relevant for this problem is also shown, typical in the Alkaline-earth-like atoms such as Sr or Yb used in OLCs.

$|\downarrow\rangle$ and $|\uparrow\rangle$ are the ground and excited states of the clock transition, respectively. To understand the quantum noise in this scenario, we describe the spin system by the collective spin operators $\hat{J}_{\alpha} = \sum_{i=1}^N \hat{j}_{\alpha}^{(i)}$, where $\hat{j}^{(i)}$ is the vector pseudospin operator describing atom i and $\hat{j}_0^{(i)}/\hbar = \mathbb{1}/2$ [39]. Rabi oscillations on the atomic transition driven by a clock laser operating as a local oscillator are governed by the rotating-frame Hamiltonian $\hat{H}_{\text{rot}} = \Omega \hat{J}_x - \delta \hat{J}_z$, where $\delta = \omega_L - \omega_0$ is the detuning of the clock laser with respect to the atomic transition and Ω is the corresponding Rabi frequency.

QND measurements are described by introducing a “meter” in the form of a pulse of light with mode operator a and thus field quadratures $\hat{X} \equiv (\hat{a}^{\dagger} + \hat{a})/2$ and $\hat{P} \equiv i(\hat{a}^{\dagger} - \hat{a})/2$, such that $[\hat{X}, \hat{P}] = i/2$. During a measurement, the meter interacts with the atoms via Hamiltonian

\hat{H}_{qnd} for time τ , such that $\tau \hat{H}_{\text{qnd}} = g \hat{n} \hat{N}_{\downarrow} \approx g |\alpha|^2 \hat{N}_{\downarrow} + 2g |\alpha| \Delta \hat{P} \hat{N}_{\downarrow}$ [40], where g is the atom-light coupling constant [42], $\hat{n} = \hat{a}^{\dagger} \hat{a}$ is the photon number operator, and $\Delta \hat{A} \equiv \hat{A} - \langle A \rangle$ indicates a deviation from the mean. The approximation follows assuming that the input pulses are coherent states, with amplitude $\alpha = i|\alpha|$ and thus $\langle X \rangle = 0$, $\langle P \rangle = |\alpha|$, $\langle n \rangle = |\alpha|^2$. We assume here that the atoms are uniformly coupled to the cavity field. The first term, which commutes with the optical variables, represents a light-shift term which induces a rotation of the atomic state about J_z , but does not contribute to the optical signal, and can be neglected [43].

The term $2g |\alpha| \Delta \hat{P} \hat{N}_{\downarrow}$ in $\tau \hat{H}_{\text{qnd}}$ contributes a phase shift $g \langle N_{\downarrow} \rangle$ to the probing light. We also assume that $g \langle N_{\downarrow} \rangle \ll \pi$, which can always be satisfied by choice of probe light detuning, and that the QND pulse duration is short compared with the Rabi dynamics $\tau \ll \pi/\Omega$. Then the postinteraction value $\hat{X}^{(\text{out})} = \hat{X}^{(\text{in})} + g |\alpha| \hat{N}_{\downarrow}$ serves as a linear “pointer” to indicate the ground state population $\hat{N}_{\downarrow} = \hat{J}_0 - \hat{J}_z$ at the time t when the pulse interacts with the atoms. A strong homodyne readout of $\hat{X}^{(\text{out})}$ completes the QND measurement.

Measurement protocol and estimation strategy.—We assume an ensemble of N atoms is prepared by optical pumping in the ground state $|\downarrow\rangle^{\otimes N}$ of the clock transition, and allow for fluctuations in the atom number due to the random processes involved in loading the trapped atoms. The clock laser drives the transition causing the spin state to execute Rabi oscillations with frequency Ω . A set of QND measurements of $\hat{X}^{(\text{out})}$ is performed at times t_l , with corresponding outcomes $\mathbf{X} \equiv \{X_l\}$, using a number of photons $|\alpha_l|^2$ in each measurement. We use \mathbf{X} to build an estimator δ_{est} for the clock laser detuning (see the Supplemental Material [40]). For large atom number N , \mathbf{X} can be well approximated by a Gaussian random variable with distribution

$$P(\mathbf{X}|\delta) = \frac{1}{\sqrt{(2\pi)^d |\Gamma_X|}} \exp\left[-\frac{1}{2}(\mathbf{X} - \boldsymbol{\mu})^T \Gamma_X^{-1} (\mathbf{X} - \boldsymbol{\mu})\right] \quad (1)$$

where d is the length of \mathbf{X} , $\boldsymbol{\mu}$ and Γ_X are the mean and covariance matrix of \mathbf{X} , respectively, which are functions of δ . After linearization about δ_0 , the nominal value of δ , and defining $\boldsymbol{\mu}_0 \equiv \boldsymbol{\mu}(\delta_0)$, the maximum likelihood estimator for δ is [40]

$$\delta_{\text{est}} = \delta_0 + \frac{(\boldsymbol{\mu}')^T \Gamma_X^{-1} (\mathbf{X} - \boldsymbol{\mu}_0)}{(\boldsymbol{\mu}')^T \Gamma_X^{-1} \boldsymbol{\mu}'}, \quad (2)$$

where $\boldsymbol{\mu}' \equiv \partial_{\delta} \boldsymbol{\mu}|_{\delta_0}$. The sensitivity of the protocol to the laser detuning δ is given by the mean squared error (MSE) of the detuning [45]:

$$\text{MSE}(\delta) \equiv E[(\delta_{\text{est}} - \delta)^2] = \frac{1}{(\boldsymbol{\mu}')^T \Gamma_X^{-1} \boldsymbol{\mu}'}. \quad (3)$$

To compute $\boldsymbol{\mu}$ and Γ_X we employ established covariance matrix methods [46–51]. We describe the spin system and optical probe pulses with the phase-space vector $\hat{\mathbf{V}} = \hat{\mathbf{J}} \oplus \left(\bigoplus_{i=1}^{N_{\text{pulses}}} \Delta \hat{\mathbf{Q}}_i \right)$, where $\hat{\mathbf{J}} = (\hat{J}_0, \hat{J}_x, \hat{J}_y, \hat{J}_z)^T$, and $\hat{\mathbf{Q}}_i \equiv (\hat{X}_i, \hat{P}_i)^T$ describes the i th optical pulse. We assume that the state is Gaussian, and remains so during the entire measurement sequence. The system is thus completely characterized by the vector of first moments $\langle \mathbf{V} \rangle$ and the covariance matrix $\Gamma_V = 1/2 \langle \mathbf{V} \otimes \mathbf{V} + (\mathbf{V} \otimes \mathbf{V})^T - \langle \mathbf{V} \rangle \otimes \langle \mathbf{V} \rangle$. $\langle \mathbf{V} \rangle$ and Γ_V evolve deterministically through the sequence of coherent Rabi oscillations generated by \hat{H}_{rot} , and sudden light-matter interactions generated by \hat{H}_{qnd} . The transformation of the state is computed by integrating $d\hat{\mathbf{V}}/dt = -i[\hat{\mathbf{V}}, \hat{H}_{\text{qnd}}]$ and dropping terms beyond first order in quantum fluctuations, to find linear input-output relations. We include the effect of loss and decoherence due to atom-photon scattering during the probing parametrized by $\eta = \eta_\gamma |\alpha|^2$, the fraction of atoms that scatter a photon due to the interaction with a probe pulse containing $|\alpha|^2$ photons with incoherent scattering rate η_γ [40]. Multipulse sequences are constructed analogously. The model gives unsightly but useful analytic results for $\boldsymbol{\mu}$ and Γ_X , which can be read off directly from $\langle \mathbf{V} \rangle$ and Γ_V [40,47,48].

Reference protocol.—The canonical Rabi sequence starts with exactly N atoms in the state $|\downarrow\rangle^{\otimes N}$, which evolve under \hat{H}_{rot} for a time t , after which a projective measurement of \hat{N}_\downarrow (or equivalently \hat{N}_\uparrow or $\hat{N}_\uparrow - \hat{N}_\downarrow$) is made. We take the precision obtained by this sequence to define the standard quantum limit (SQL) of a Rabi-spectroscopy OLC. An equivalent protocol can be implemented using our formalism as follows: the initial state $|\downarrow\rangle^{\otimes N}$ implies $\langle \mathbf{J} \rangle = (1, 0, 0, -1)\langle N \rangle/2$, with $\Gamma_J = \text{diag}(0, 1, 1, 0)\langle N \rangle/2$. The evolution under \hat{H}_{rot} induces a δ -parametrized O(3) rotation (the \hat{J}_0 component is unchanged) of $\langle \mathbf{J} \rangle$ and Γ_J , while the measurement is of $\hat{J}_0 - \hat{J}_z$. The resulting MSE from Eq. (3) is $\text{MSE}^{\text{(SQL)}} = \kappa_1 N^{-1} + \kappa_2 (g|\alpha|^2 N)^{-1}$, where κ_1, κ_2 are constants that depend on the chosen sequence parameters Ω, δ .

Three-pulse protocol.—The new protocol includes three QND measurement pulses. The ensemble of atoms is prepared in the ground state $|\downarrow\rangle^{\otimes N}$, and we allow for Poisson-distributed atom number fluctuations in the input state [52]. The state is then allowed to evolve under \hat{H}_{rot} and subject to QND measurements at times $t_1 = 0$, i.e., immediately after state preparation, t_2 and t_3 , with the number of photons per measurement pulse $|\alpha_1|^2, |\alpha_2|^2, |\alpha_3|^2$. In essence, the first QND pulse is used to calibrate the number of atoms, while the other two act as squeezing and read-out

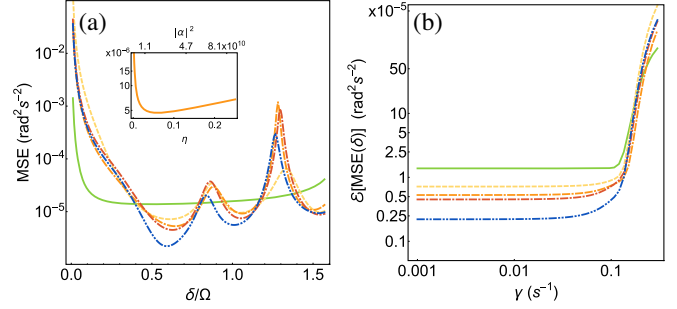


FIG. 2. (a) Sensitivity of the QND measurement protocol. Curves show the MSE of the detuning δ as a function of the drive laser detuning δ , as per Eq. (3). Atom number is $N = 2 \times 10^4$, atom-light coupling $g \simeq 3.05 \times 10^{-7}$ rad/atom obtained for an intracavity power of $\simeq 4$ mW. The solid green curve shows the results for the reference protocol described in the main text, defining the standard quantum limit. The dashed yellow curve shows the three-measurement protocol with $t_1 = \pi/\Omega$, $t_2 = 3\pi/\Omega$ (*a priori* values) and $|\alpha_1|^2 = |\alpha_2|^2 = |\alpha_3|^2 = |\alpha_{\text{ref}}|^2 = 7.18 \times 10^9$ (found by minimization of MSE with respect to $|\alpha_{\text{ref}}|^2$). The dashed-dashed-dot orange curve shows the three-measurement protocol with measurement timings $t_1 = 0$, $t_2 \approx 1.79\pi/\Omega$, and $t_3 \approx 3\pi/\Omega$, (found by optimization of MSE with respect to t_i) and keeping the values for $|\alpha_1|^2 = |\alpha_2|^2 = |\alpha_3|^2 = |\alpha_{\text{ref}}|^2 = 7.14 \times 10^9$. The dot-dashed red curve shows the three-measurement protocol found by optimization of the timings and the number of photons per measurement pulse while keeping the total equal to the previous protocol, i.e., $|\alpha_1|^2 + |\alpha_2|^2 + |\alpha_3|^2 \leq 3|\alpha_{\text{ref}}|^2$. In this case, $t_2 \approx 1.27\pi/\Omega$, $t_3 \approx 3\pi/\Omega$, and $|\alpha_1|^2 = 3.37 \times 10^9$, $|\alpha_2|^2 = 5.4 \times 10^9$, $|\alpha_3|^2 = 1.28 \times 10^{10}$. The dot-dot-dashed blue curve shows a full optimization of the timings and number of photons without the previous constraint, with optimum parameters $t_2 \approx 1.29\pi/\Omega$, $t_3 \approx 3\pi/\Omega$, and $|\alpha_1|^2 = 9.77 \times 10^9$, $|\alpha_2|^2 = 2.12 \times 10^{10}$, $|\alpha_3|^2 = 1.35 \times 10^{11}$. Inset: the MSE with the timings corresponding to the orange protocol (i.e., same measurement timing, and equal measurement pulses) at the optimum detuning $\delta_0/\Omega \simeq 0.6$ for varying measurement strength (photon number for each measurement pulse) parametrized by the fraction of atoms η that suffers incoherent scattering during the protocol. (b) Numerical results of the averaged single shot estimator variance $E[\text{MSE}(\delta)]$ as defined in the main text as a function of the clock laser phase noise parameter γ , with the same color coding as in panel (a).

pulses. The δ -dependent MSE is calculated using Eq. (3), optimized with respect to measurement times t_i and photon numbers $|\alpha_i|^2$.

Sensitivity optimization and clock stability.—Figure 2(a) shows the sensitivity of our reference protocol as a function of the driving laser detuning δ using different parameters for a typical atom number $N = 2 \times 10^4$. Each dashed line corresponds to a different choice of settings $\{|\alpha_i|^2, t_i\}$, found by minimizing $\text{MSE}(\delta)$ with respect to δ and $\{|\alpha_i|^2, t_i\}$, subject to constraints on $\{|\alpha_i|^2, t_i\}$, e.g., $\sum_i |\alpha_i|^2 = |\alpha_{\text{tot}}|^2$ [see caption in Fig. 2(a)]. With *a priori* timing of the measurements and optimized photon

numbers, we observe an improvement in the sensitivity of ~ 2.8 dB with respect to the SQL. With further optimization of the pulse timings an improvement of ~ 4.2 dB relative to the SQL is achieved, and when both timing and measurement strength (i.e., photon number) are fully optimized, the protocol achieves ~ 7.9 dB improvement over the SQL.

Allan variance.—Current state-of-the-art OLCs are limited by the DE rather than the QPN. Nevertheless, there are situations where the enhanced sensitivity of the proposed protocol will be advantageous. For instance, synchronous clock comparison measurements allow one to access the QPN-limited precision, and are important in precision measurements for fundamental tests, accurate measurements of fundamental constants, geodesy, or searches of exotic physics [5,6,53–55]. In addition, the functional relation of the sensitivity with respect to the detuning in our protocol differs from that of a standard clock protocol. In all these situations, it becomes important to assess the quality of our estimation taking into account the random phase fluctuations of the driving clock laser. The corresponding Allan deviation of the fractional frequency instability of an OLC using our protocol can be written as $\sigma^2(\tau_{\text{av}}) = \mathcal{E}[\text{MSE}(\delta)]T_c/(\omega_0^2\tau_{\text{av}})$ [56,57], where T_c is the cycling time of the clock, and τ_{av} is the averaging time, ω_0 is the atomic clock transition frequency, and

$$\mathcal{E}[\text{MSE}(\delta)] = \int_{\delta_{\text{est}}-\varepsilon}^{\delta_{\text{est}}+\varepsilon} dP_\gamma(\delta)\text{MSE}(\delta), \quad (4)$$

where $P_\gamma(\delta) = 1/(\gamma\sqrt{2\pi})\exp[-(\delta_{\text{est}} - \delta)^2/2\gamma^2]$ is the probability density for the random variable δ for a clock laser with a one sided power spectral density $S(\nu) = 2\gamma^2/\nu$, which models current state-of-the-art clock lasers in which the dominant source of noise is flicker noise [58,59]. To avoid including unphysical divergences in the integral, we take $\varepsilon = \pi\Omega$ [60]. The expression for $\sigma^2(\tau_{\text{av}})$ does not include the effect of dead time in the clock cycle. Figure 2(b) shows the results of computing the averaged single shot estimator variance $\mathcal{E}[\text{MSE}(\delta)]$ as a function of the laser noise parameter γ for the different curves in Fig. 2(a). The different configurations of the three-measurement protocol show consistent improvement with respect to the reference protocol for a wide range of laser noise parameters $\gamma < 0.1$ [40], within current experimental capabilities of clock lasers [7].

Measurement back action and spin squeezing.—Entanglement among the atoms can be detected using spin-squeezing inequalities [61] that constrain the statistics of $\hat{\mathbf{J}}$. In particular, if $\{\hat{J}_j, \hat{J}_k, \hat{J}_l\}$ are orthogonal components of $\hat{\mathbf{J}}$, all separable states with uncertain particle number obey several spin-squeezing inequalities [40,62]. In the large- N scenario, we can define a witness [40]:

$$\xi^2 \equiv \min_{\{j,k,l\}} \frac{\langle N \rangle \langle \Delta \hat{J}_l \rangle^2}{\langle \hat{J}_j \rangle^2 + \langle \hat{J}_k \rangle^2}, \quad (5)$$

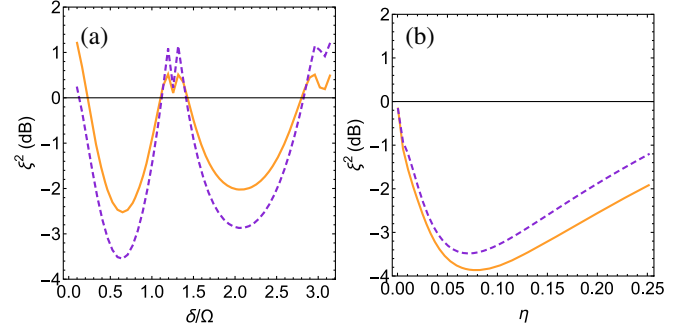


FIG. 3. Numerical evaluation of the spin-squeezing witness ξ^2 in Eq. (5) using the three-measurement protocol with equal number of photons per measurement, as in the dot-dashed orange curve of Fig. 2. We plot ξ^2 as a function of (a) the clock laser detuning δ for the same protocol with two different numbers of photons per measurement $|\alpha|^2 = \{7.18 \times 10^9, 2 \times 7.18 \times 10^9\}$ and (b) the measurement strength for two different detunings $\delta/\Omega = \{0.642, 0.5\}$. In both plots the orange line corresponds to the parameters giving the optimized clock sensitivity, and the dashed purple curve shows the same protocol with different parameters.

where $\{\hat{j}, \hat{k}, \hat{l}\}$ are orthonormal. $\xi^2 < 1$ indicates the presence of spin squeezing and entanglement.

In Fig. 3 we plot ξ^2 immediately prior to the third QND measurement of the three-measurement protocol using the same number of photons per measurement (as in the orange line in Fig. 2) as a function of the clock laser detuning and measurement strength. While the qualitative behavior of the entanglement witness is similar to that of the clock sensitivity, we note that it is not a reliable indicator of the optimum sensitivity. In Fig. 3(a) we can see how choosing a different measurement strength leads to larger squeezing of the atomic state, while this configuration is not the optimum for the protocol sensitivity. This is not unexpected, since the witness does not capture correlations due to the coupling of \hat{J}_0 into the QND measurement. Using a spin-squeezing witness which could account for the correlations between \hat{J}_0 and the other spin variables would be desirable. However, to the best of our knowledge, such witness has not been presented in the literature.

Conclusions and outlook.—In this Letter, we propose and analyze a minimal three pulse QND-based measurement protocol directly applicable to state-of-the-art OLCs using Rabi protocols and limited by QPN. By exploiting a multimeasurement estimation strategy and measurement induced correlations, we show a 7.9 dB enhanced single shot sensitivity of the clock with respect to the SQL for $N = 2 \times 10^4$ atoms. Our calculation techniques allow for straight-forward optimization of relevant experimental parameters, such as the timing and strength of each QND measurement. Using an entanglement witness derived from spin-squeezing inequalities for a fluctuating atom number, we infer that the protocol generates entanglement.

The proposed protocol can improve the short-term stability of clock experiments that include strategies to evade the DE using multiple ensembles and synchronous measurement [2,9–11], and could be combined with spin-echo protocols to counteract inhomogeneous broadening induced by nonuniform atom-light coupling [26]. Possible extensions of the framework presented here can extend the Gaussian description of the system to include diffusion terms [63], naturally incorporating into the results the noise characteristics of the clock laser. We leave for future work the question of whether similar protocols with additional measurements, continuous probing, and/or controlled phase shifts in the drive laser could give further enhancement.

This work was supported by the European Union from the European Metrology Programme for Innovation and Research (EMPIR) Project No. 17FUN03-USOQS. EMPIR projects are cofunded by the European Union’s Horizon 2020 research and innovation program and the EMPIR participating states. We also acknowledge H2020 QuantERA ERA-NET Cofund Q-CLOCKS (PCI2018-092973 project funded by MCIN/AEI/FEDER “A way to make Europe”), H2020 FET Quantum Technologies Flagship project MACQSIMAL (Grant No. 820393), the Spanish Ministry of Science projects OCARINA (PGC2018-097056-B-I00 project funded by MCIN/AEI/FEDER “A way to make Europe”) and “Severo Ochoa” Center of Excellence CEX2019-000910-S. Generalitat de Catalunya: CERCA, AGAUR Grant No. 2017-SGR-1354, Secretaria d’Universitats i Recerca (project QuantumCat, Ref. No. 001-P-001644), Fundació Privada Cellex, and Fundació Mir-Puig.

[1] N. Hinkley, J. A. Sherman, N. B. Phillips, M. Schioppo, N. D. Lemke, K. Beloy, M. Pizzocaro, C. W. Oates, and A. D. Ludlow, *Science* **341**, 1215 (2013).
 [2] E. Oelker, R. Hutson, C. Kennedy, L. Sonderhouse, T. Bothwell, A. Goban, D. Kedar, C. Sanner, J. Robinson, G. Marti *et al.*, *Nat. Photonics* **13**, 714 (2019).
 [3] N. Huntemann, B. Lipphardt, C. Tamm, V. Gerginov, S. Weyers, and E. Peik, *Phys. Rev. Lett.* **113**, 210802 (2014).
 [4] C. Lisdat *et al.*, *Nat. Commun.* **7**, 12443 (2016).
 [5] M. Takamoto, I. Ushijima, N. Ohmae, T. Yahagi, K. Kokado, H. Shinkai, and H. Katori, *Nat. Photonics* **14**, 411 (2020).
 [6] M. S. Safronova, D. Budker, D. DeMille, Derek F. Jackson J. Kimball, A. Derevianko, and C. W. Clark, *Rev. Mod. Phys.* **90**, 025008 (2018).
 [7] M. Schulte, C. Lisdat, P. O. Schmidt, U. Sterr, and K. Hammerer, *Nat. Commun.* **11**, 5955 (2020).
 [8] M. A. Norcia, A. W. Young, W. J. Eckner, E. Oelker, J. Ye, and A. M. Kaufman, *Science* **366**, 93 (2019).
 [9] M. Takamoto, T. Takano, and H. Katori, *Nat. Photonics* **5**, 288 (2011).

[10] M. Schioppo, R. C. Brown, W. F. McGrew, N. Hinkley, R. J. Fasano, K. Beloy, T. H. Yoon, G. Milani, D. Nicolodi, J. A. Sherman, N. B. Phillips, C. W. Oates, and A. D. Ludlow, *Nat. Photonics* **11**, 48 (2017).
 [11] T. L. Nicholson, M. J. Martin, J. R. Williams, B. J. Bloom, M. Bishof, M. D. Swallows, S. L. Campbell, and J. Ye, *Phys. Rev. Lett.* **109**, 230801 (2012).
 [12] J. Lodewyck, P. G. Westergaard, and P. Lemonde, *Phys. Rev. A* **79**, 061401(R) (2009).
 [13] M.-Z. Huang, Spin squeezing and spin dynamics in a trapped-atom clock, thesis, Sorbonne Université, 2019.
 [14] E. S. Polzik and J. Ye, *Phys. Rev. A* **93**, 021404(R) (2016).
 [15] R. J. Sewell, M. Napolitano, N. Behbood, G. Colangelo, and M. W. Mitchell, *Nat. Photonics* **7**, 517 (2013).
 [16] T. Takano, M. Fuyama, R. Namiki, and Y. Takahashi, *Phys. Rev. Lett.* **102**, 033601 (2009).
 [17] J. Appel, P. J. Windpassinger, D. Oblak, U. B. Hoff, N. Kjærgaard, and E. S. Polzik, *Proc. Natl. Acad. Sci. U.S.A.* **106**, 10960 (2009).
 [18] R. J. Sewell, M. Koschorreck, M. Napolitano, B. Dubost, N. Behbood, and M. W. Mitchell, *Phys. Rev. Lett.* **109**, 253605 (2012).
 [19] O. Hosten, N. J. Engelsen, R. Krishnakumar, and M. A. Kasevich, *Nature (London)* **529**, 505 (2016).
 [20] V. Braginsky and Y. Vorontsov, *Usp. Fiz. Nauk* **114**, 41 (1974).
 [21] G. Vasilakis, V. Shah, and M. V. Romalis, *Phys. Rev. Lett.* **106**, 143601 (2011).
 [22] G. Vasilakis, H. Shen, K. Jensen, M. Balabas, D. Salart, B. Chen, and E. S. Polzik, *Nat. Phys.* **11**, 389 (2015).
 [23] G. Colangelo, F. M. Ciurana, L. C. Bianchet, R. J. Sewell, and M. W. Mitchell, *Nature (London)* **543**, 525 (2017).
 [24] N. Shiga and M. Takeuchi, *New J. Phys.* **14**, 023034 (2012).
 [25] R. Kohlhaas, A. Bertoldi, E. Cantin, A. Aspect, A. Landragin, and P. Bouyer, *Phys. Rev. X* **5**, 021011 (2015).
 [26] W. Bowden, A. Vianello, I. R. Hill, M. Schioppo, and R. Hobson, *Phys. Rev. X* **10**, 041052 (2020).
 [27] M. H. Schleier-Smith, I. D. Leroux, and V. Vuletić, *Phys. Rev. Lett.* **104**, 073604 (2010).
 [28] J. G. Bohnet, K. C. Cox, M. A. Norcia, J. M. Weiner, Z. Chen, and J. K. Thompson, *Nat. Photonics* **8**, 731 (2014).
 [29] M. G. Tarallo, D. Calonico, F. Levi, M. Barbiero, G. Lamporesi, and G. Ferrari, in *2017 Joint Conference of the European Frequency and Time Forum and IEEE International Frequency Control Symposium (EFTF/IFCS)* (IEEE, 2017), pp. 748–750, 10.1109/FCS.2017.8089020.
 [30] W. Bowden, R. Hobson, I. R. Hill, A. Vianello, M. Schioppo, A. Silva, H. S. Margolis, P. E. G. Baird, and P. Gill, *Sci. Rep.* **9**, 11704 (2019).
 [31] G. Vallet, E. Bookjans, U. Eismann, S. Bilicki, R. L. Targat, and J. Lodewyck, *New J. Phys.* **19**, 083002 (2017).
 [32] A. Kuzmich, N. P. Bigelow, and L. Mandel, *Europhys. Lett.* **42**, 481 (1998).
 [33] L. K. Thomsen, S. Mancini, and H. M. Wiseman, *J. Phys. B* **35**, 4937 (2002).
 [34] Z. Chen, J. G. Bohnet, J. M. Weiner, K. C. Cox, and J. K. Thompson, *Phys. Rev. A* **89**, 043837 (2014).
 [35] A. Louchet-Chauvet, J. Appel, J. J. Renema, D. Oblak, N. Kjaergaard, and E. S. Polzik, *New J. Phys.* **12**, 065032 (2010).

- [36] R. Hobson, W. Bowden, A. Vianello, I. R. Hill, and P. Gill, *Opt. Express* **27**, 37099 (2019).
- [37] D. Meiser, J. Ye, and M. J. Holland, *New J. Phys.* **10**, 073014 (2008).
- [38] E. Pedrozo-Peñañiel, S. Colombo, C. Shu, A. F. Adiyatullin, Z. Li, E. Mendez, B. Braverman, A. Kawasaki, D. Akamatsu, Y. Xiao, and V. Vuletić, *Nature (London)* **588**, 414 (2020).
- [39] From now and throughout the rest of the work, we set $\hbar = 1$. Vectors are written in bold characters, while components of vectors use normal italic notation. Mean field values of operators $\hat{\mathcal{O}}$ are indicated using bracket $\langle \mathcal{O} \rangle$ notation.
- [40] See Supplemental Material at <http://link.aps.org/supplemental/10.1103/PhysRevLett.128.153201>, contains mathematical proofs and details which are relevant for the methods used in the calculations described within the manuscript, which includes Ref. [41].
- [41] M. Koschorreck, M. Napolitano, B. Dubost, and M. W. Mitchell, *Phys. Rev. Lett.* **104**, 093602 (2010).
- [42] $g = (1/S_{\text{eff}})(3\lambda^2/2\pi)\{(\Delta_{\text{qnd}}/\Gamma)/[s + 4(\Delta_{\text{qnd}}/\Gamma)^2]\}$, with s a saturation parameter that depends on the intracavity power and S_{eff} an effective geometric coupling parameter. In this formula Δ_{qnd} is the probe light detuning with respect to the atomic transition. Realistic experimental parameters have been chosen according to [31].
- [43] The effect of this term can be canceled by precise control of the optical power and coupling constant, i.e., by making $g|\alpha|^2 = 2\pi j$, $j \in \mathbb{Z}$ [33], or by adapting more sophisticated optical probing techniques [44].
- [44] M. Saffman, D. Oblak, J. Appel, and E. S. Polzik, *Phys. Rev. A* **79**, 023831 (2009).
- [45] In case of maximum likelihood, unbiased estimators, the MSE is equivalent to the estimator variance. The proof that our estimator is unbiased can be found in the Supplemental Material.
- [46] L. B. Madsen and K. Mølmer, *Phys. Rev. A* **70**, 052324 (2004).
- [47] M. Koschorreck and M. W. Mitchell, *J. Phys. B* **42**, 195502 (2009).
- [48] G. Colangelo, R. J. Sewell, N. Behbood, F. M. Ciurana, G. Triginer, and M. W. Mitchell, *New J. Phys.* **15**, 103007 (2013).
- [49] B. Kraus, K. Hammerer, G. Giedke, and J. I. Cirac, *Phys. Rev. A* **67**, 042314 (2003).
- [50] K. Mølmer and L. B. Madsen, *Phys. Rev. A* **70**, 052102 (2004).
- [51] V. Petersen and K. Mølmer, *Phys. Rev. A* **74**, 043802 (2006).
- [52] G. Colangelo, F. Martin Ciurana, G. Puentes, M. W. Mitchell, and R. J. Sewell, *Phys. Rev. Lett.* **118**, 233603 (2017).
- [53] R. Lange, N. Huntemann, J. M. Rahm, C. Sanner, H. Shao, B. Lipphardt, C. Tamm, S. Weyers, and E. Peik, *Phys. Rev. Lett.* **126**, 011102 (2021).
- [54] R. M. Godun, P. B. R. Nisbet-Jones, J. M. Jones, S. A. King, L. A. M. Johnson, H. S. Margolis, K. Szymaniec, S. N. Lea, K. Bongs, and P. Gill, *Phys. Rev. Lett.* **113**, 210801 (2014).
- [55] T. Takano, M. Takamoto, I. Ushijima, N. Ohmae, T. Akatsuka, A. Yamaguchi, Y. Kuroishi, H. Munekane, B. Miyahara, and H. Katori, *Nat. Photonics* **10**, 662 (2016).
- [56] D. Allan, *Proc. IEEE* **54**, 221 (1966).
- [57] L. Pezzé and A. Smerzi, *Phys. Rev. Lett.* **125**, 210503 (2020).
- [58] B. Braverman, A. Kawasaki, and V. Vuletić, *New J. Phys.* **20**, 103019 (2018).
- [59] A. André, A. S. Sørensen, and M. D. Lukin, *Phys. Rev. Lett.* **92**, 230801 (2004).
- [60] Due to the linearization leading to Eq. (2), $\text{MSE}(\delta)$, valid near $\delta = \delta_{\text{est}}$, diverges near $\delta = \delta_0$. As a check on the approach of limiting the integral to $\delta_{\text{est}} \pm \varepsilon$, we follow [58] and integrate over all δ the regularized $\widetilde{\text{MSE}}(\delta) \equiv \min[\text{MSE}(\delta), 4 \text{ rad}^2 \text{ s}^{-2}]$, where $4 \text{ rad}^2 \text{ s}^{-2}$ is an upper bound on the uncertainty in light of the linewidth. The results are consistent with the simpler method used here.
- [61] G. Tóth, C. Knapp, O. Gühne, and H. J. Briegel, *Phys. Rev. Lett.* **99**, 250405 (2007).
- [62] P. Hyllus, L. Pezzé, A. Smerzi, and G. Tóth, *Phys. Rev. A* **86**, 012337 (2012).
- [63] M. G. Genoni, L. Lami, and A. Serafini, *Contemp. Phys.* **57**, 331 (2016).